Accepted Manuscript

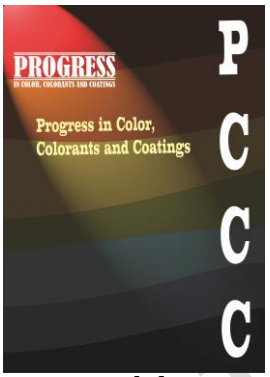

Title: Preparation of a hybrid pigment by the adsorption of Alizarin Red S dye on mesoporous silica for the removal and detection of heavy metals

Authors: Sara Chabokrow, Kamaladin Gharanjig, Narges Yousefi-Limaee, Mehdi Ghahari1Yari

Manuscript number**: PCCC-2512-1484**

To appear in: Progresss in Color, Colorants and Coatings

Received: 28 December 2025

Final Revised: 23 April 2026

Accepted: 27 April 2026

Please cite this article as:

S. Chabokrow, K. Gharanjig, N. Yousefi-Limaee, M. Ghahari, Preparation of a hybrid pigment by the adsorption of Alizarin Red S dye on mesoporous silica for the removal and detection of heavy metals, Prog. Color, Colorants, Coat., 20 (2027) XX-XXX.

DOI: 10.30509/pccc.2026.167749.1484

Preparation of a hybrid pigment by the adsorption of Alizarin Red S dye on mesoporous silica for the removal and detection of heavy metals

S. Chabokrow[1], K. Gharanjig[2], N. Yousefi-Limaee[3], M. Ghahari[1,*]

1- Department of Nanomaterials and Nanocoatings, Institute for Color Science and Technology, P.O. Box: 16765-654,Tehran, Iran.

2- Department of Organic Colorants, Institute for Color Science and Technology, Tehran, P.O. Box 16656118481, Iran

3- Department of Environmental Research, Institute for Color Science and Technology, P.O. Box: 16765-654, Tehran, Iran.

* Corresponding author E-mail: maghahari@icrc.ac.ir

Abstract

Heavy metal contamination in aqueous media poses significant risks to environmental and human health. Effective removal of these contaminants from water sources is crucial to safeguard ecosystems, ensure safe drinking water, and prevent bioaccumulation in food chains. This study focused on the synthesis of a hybrid pigment by combining an organic and an inorganic component. The resulting pigments exhibited the capacity to absorb metal ions. Notably, for the first time, a Silica-Alizarin Red S hybrid pigment (SC-ARS) was developed using porous silica powder. This hybrid pigment was evaluated for its effectiveness in removing heavy metals, including lead (Pb(II)), copper (Cu(II)), and cadmium (Cd(II)), from aqueous media. The synthesis process comprised three key steps: The initial step involved synthesizing the mineral component using the Stöber method and characterizing its surface properties and morphology. The second step

focused on functionalizing the material to develop the SC-ARS hybrid pigment and on optimizing the binding of Alizarin Red S to the silica substrate. Finally, a thorough investigation was conducted to identify the optimal conditions for Alizarin Red S adsorption. The results indicated that the maximum adsorption capacity was achieved at 298 K, pH 5, an initial dye concentration of 5 g/L, 0.04 g of adsorbent, and a contact time of 10 minutes. The SC-ARS pigment exhibited notable removal efficiencies for heavy metal ions, achieving 96% removal for Cu(II), 84% for Cd(II), and 99% for Pb(II) from aqueous solutions, as confirmed by ICP analysis. This outcome emphasizes its potential as an effective adsorbent for environmental applications. The potential industrial applications of these hybrid materials include wastewater treatment, environmental remediation, water filtration systems, chemical manufacturing, coatings and paints, agricultural applications, and electronics and battery production.

Keywords: Hybrid Pigment, mesoporous Silica, Alizarin Red S, Heavy metal ions, Langmuir , pseudo-second-order.

1. Introduction

Heavy metal ions, including copper, cadmium, and lead, are harmful to the environment and human health even at relatively low concentrations because they can be persistent in vital human organs and transferred into an organism's chain as well as accumulating in living organisms [1, 2]. Therefore, by advancing the technology, scientists have worked on new types of material such as organic or inorganic compounds to produce hybrid materialsdue toestablishing chemical and physical connection between organic and

inorganic components[3-5]. There is a variety of approaches to reduce the concentration of these contaminants in aqueous systems, such as precipitation [6], filtration [7], ion exchange [8], reverse osmosis [9], and adsorption [10]. Among all existing methods, adsorption has substantial advantages, including the efficient removal of metal ions with low energy expense and appropriate selectivity [11, 12]. The adsorption can be improved by surface functionalization of adsorbent with a particular surfactant [13, 14]. Alizarin Red S (ARS) is an anionic anthraquinone dye known for its electrochemical and spectrophotometric properties, making it useful as a surface-functionalizing agent. This synthetic colorant is commonly employed in the textile industry; however, it also poses a significant environmental concern as a persistent pollutant in aquatic ecosystems [15]. It can enhances the bonding between heavy metal ions including Cu (II), Cd (II) and Pb (II) and negatively charged material.

Mesoporous silica materials are characterized by their ordered porous structures, extensive surface areas, and tunable pore sizes, which render them exceptionally effective for a range of applications, including adsorption. The functionalization of ordered mesoporous silica with organic or hybrid functional groups opens up new avenues for optimizing their chemical, physical, and mechanical properties [16]. Hybrid materials, which integrate both organic and inorganic components, exhibit synergistic properties that significantly enhance the adsorption of heavy metal ions. These materials can be specifically designed with functional groups that effectively chelate heavy metal ions [17]. Furthermore, Cetyltrimethylammonium bromide (CTAB) is a cationic surfactant widely used for modifying materials [18]. The incorporation of CTAB during the synthesis process enhances the interaction between the anionic dye Alizarin Red S and

the porous silica. As a result, the material can be regarded as hybrid in two respects: 1) the bonding of CTAB to the O-Si-O framework, and 2) the chemical bond formation between Alizarin Red S and CTAB.

In recent decades, the adsorption kinetics of organic material has been considered on porous silica [19]. Zaggout et al. investigated the adsorption kinetics of ARS on silica surface [20]. Also, modification of silica surface with gamma aminopropyltrioethoxysilane was carried out by Li et al. as well as investigation the adsorption of ARS on modified silica [21]. Li et al. have prepared the hybrid material from the silica gel and ARS to adsorb various ions, including Cu (II) and Cd (II) extracted from rice and water [22].

Due to wide application of porous silica powder in the adsorption, the aim of this study was first to synthesis porous silica followed by surface functionalization by cationic surfactant. As a result, porous silica with a high surface area was synthesized by the modified Stober method. Afterwards, the synthesized silica was bonded toARS dye to make a hybrid pigment. The optimization factors including time, pH, concentration, adsorbent dosage and temperature was investigated for adsorbing the dye. At last, this hybrid materials were used for the adsorption of metal ions.

2. Experimental

2.1. Materials

This study aimed to investigate the effect of surface area and surface treatment of silica on its removal capability. The Stober and modified sol-gel processes were utilized to synthesize silica material to examine the effect of surface area. Additionally, the effect of

Alizarin Red S (ARS) on silica's surface was studied. In this regard, Cetyltrimethylammonium bromide (CTAB) >98%, Alizarin Red S> 95%, and NaOH>%98 was provided from Merck and Tetraethyl orthosilicate (TEOS) >98% was purchased from Daejung Chemicals. All of the materials were used without any further purification. The pH adjustment was carried out with HCl and NaOH purchased from Merck. The salts of $Pb(NO_3)_2$, $Cu(NO_3)_2$, and $CdCl_2$ were used to study the adsorption of heavy metal ions on the adsorbent and purchased from Merck.

2.2. Synthesis of the silica particles by stober (S) method

To prepare silica powder using the Stober method, 4 mL of ammonia was added to one container, while another containing 20 mL of ethanol was added with 4 mL of distilled water. Next, 1.6 mL of silica precursor (TEOS) was mixed with 14 mL of ethanol in the second container. Then, the contents of the second container were slowly added to the first container while stirring at 500 rpm for one hour at room temperature. After one hour, the white silica powder was separated from the mixture and washed with water and ethanol [23].

2.3. Synthesis of the silica particles by modified stober method (SCT & SC)

To synthesize porous silica using the modified Stober method, 0.5 g of CTAB cationic surfactant was dissolved in 150 mL of distilled water at 353K. The Critical Micelle Concentration (CMC) of CTAB is approximately 0.32 gL^{-1}, but 1.93 gL^{-1} of CTAB was used in this study to form more micelles and create more pores. After the formation of CTAB micelles in the aqueous medium, 0.29 g of pentanol and 1 mL of NaOH (2 M)

were added to the solution to bring the pH to 12. Then, 0.8 mL of TEOS was added as a source of silica. The silica particles formed and grew gradually after 2 hours at 80°C. After synthesis, the particles were filtered and washed seven times with distilled water to remove extra CTAB. Ultimately, CTAB functionalized porous silica (SC) was prepared using the cationic surfactant [1].

The presence of surfactant within the porous silica pores makes the exact volume and diameter values of the pores and the wall between them unclear. In order to address this, the functionalized silica particles (SC) were heat treated at 500°C for 5 hours to eliminate the surfactant. The thermal treatment sample (SCT) was conducted to clarify the size and volume of the pores and the wall separating them.

Based on the results obtained from the adsorption of ARS dye by the synthesized adsorbents (S, SC, and SCT), the SC adsorbent showed the highest adsorption process, while the S adsorbent had the lowest. As a result, further adsorption experiments were conducted using the SC adsorbent.

2.4. Preparation the hybrid of SC silica and ARS dye (SC-ARS)

A simple mixing procedure was applied to synthesize the desired hybrid material and create physical and chemical bonds between dye and silica. For this purpose, 0.3 g L^{-1} of the dye solution was prepared by dissolving ARS dye in distilled water. Then 0.25 g of adsorbent was separately dispersed by sonicating in 87 mL of distilled water, followed by adding 13 mL of Alizarin solution to the adsorbent dispersion. Finally, the hybrid powders are separated, filtered, and washed three times with distilled water.

2.5. Removing Heavy Metal by SC-ARS Hybrid Sorbent

The removal capability of synthesized hybrid material (SC-ARS) was investigated for the removal of Pb^{2+}, Cu^{2+}, and Cd^{2+}. For this purpose, 0.3 g of the SC-ARS hybrid material was dispersed into 150 mL of water for the adsorption of metal ions (5 mL) with a concentration of 15 ppm. After agitation for 35 min, the SC-ARS particles were separated by centrifugation, and ICP analyzed the residual solution to investigate the removal of metal ions by SC-ARS.

3. Results and Discussion

3.1. Characterization

The porosity and the surface area of adsorbent materials are essential to estimate their removal capability. In this regard, the BET analysis (or adsorption-desorption of nitrogen) was used to determine the porosity of synthesized particles. The adsorption-desorption of nitrogen gas is examined at the temperature of 77 K for three samples, namely, S, SC, and SCT. According to the patterns provided by IUPAC, the isotherm of gas adsorption on S, SC, and SCT silica samples belongs to types III, V, and IVa, respectively. A high degree of porosity with high hysteresis and a low degree of porosity with low hysteresis are attributed to the IVa and V categories, respectively [24, 25]. The results showed that S and SCT samples represent the lowest and the highest porosity, respectively. The presence of CTAB in the SC sample is probably responsible for loading the silica pores. Therefore, the porosity could be reduced compared to the SCT sample. Meanwhile, after heat treatment of the SC sample at 773K for an hour (SCT sample), the CTAB on the pores is degraded, and the actual porosity is achieved.

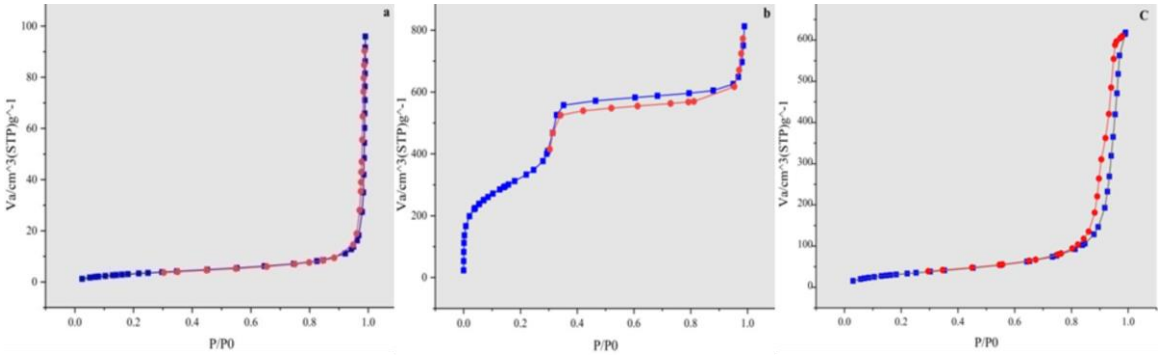

Figure 1. Diagram of adsorption-desorption of nitrogen on samplesa :S, b: SCT ,C: SC.

Also, specific surface area (ABET), total pore volume (V_t), primary pore volume (V_P), pore diameter (calculated by the mathematical method) (W_d), wall thicknesses between cavities(calculated by mathematical method) (b_d), pore diameter (calculated by BJH method)(WKJS), the maximum of Bragg angle and crystallography of synthesized silica samples were identified by BET and XRD experiments.

Equations 1 and 2 were used to calculate Wd and bd; as d_{100} is the distance between the two layers and the density of the porous wall, nr is the initial porosity volume, and C is the equation's constant.

$$Wd = cd100\left(\frac{\rho.vp}{1+\rho.vp}\right)^{\frac{1}{2}} \qquad (1)$$

$$bd = a - wd \quad \text{و} \quad a = \left(\frac{2}{3}\right)^{\frac{1}{2}} * d100 \qquad (2)$$

However, to simplify the equation, the shape of the particles was considered spherical. Consequently, r and C for the spherical pores attained 2.2 and 1.213 g cm^{-3}, respectively. The shape of the synthesized pores is another result of the diagrams of adsorption-desorption of nitrogen gas. According to the IUPAC classification, SCT silica has approximate cylindrical pores.

Table 1. The BET constants for three samples of SC, SCT, S.

Sample	A_{BET} (m^2/g)	V_m (cm^3/g)	W_{KJS} (nm)	V_p (cm^3/g)	W_d (nm)	b_d (nm)	d100 (nm)
S	13.308	3.057	-	0.14	-	-	-
SC	125.58	28.85	-	0.98	-	-	-
SCT	1174.2	269.78	4.28	1.32	4.09	0.36	3.85

According to these values, the high specific surface area and specific volume of SCT silica compared to S silica is attributed to the presence of CTAB surfactant and pentanol as a co-surfactant for synthesizing silica porous materials. Figure 2 displays the X-ray diffraction patterns of the SCT silica powder, measured at 0-10˚ and 10-40˚ degrees. These results confirm the proper synthesis of silica using the modified Stober method and reveal the hexagonal structure of the silica powder (Figure 2). The small-angle diffraction pattern (0-10˚) provides evidence of the porosity of the synthesized silica and helps determine the diameter and wall of the pores (Figure 2a). The figure also confirms that the SCT sample pattern resembles mesoporous silica with a pore structure [24].

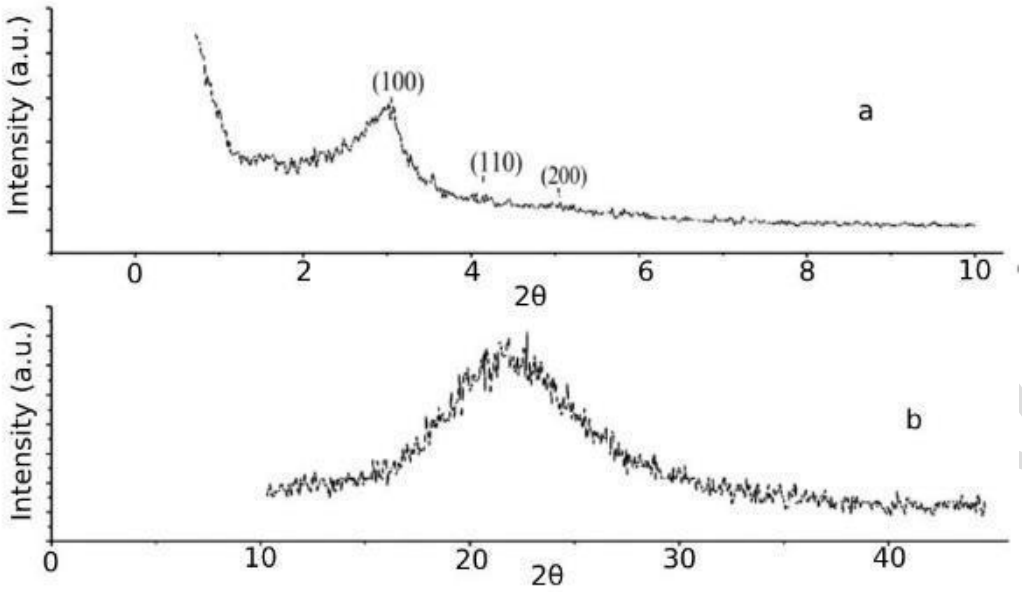

Figure 2. X-ray diffraction pattern of SCT silica powder in a) 0˚-10˚ and b)10˚-40˚

Furthermore, the high-angle pattern (Figure 2b) confirms that the synthesized silica is amorphous [26]. As shown in Figure 2a, three XRD peaks are observed at a small angle of 3.06, 4.14, and 5.12, which can be indexed as (100), (110), and (200), representing the highly ordered hexagonal mesostructure. The results indicated that the micelle diameter and volume were increased due to the presence of pentanol as the co-surfactant in the synthesis procedure. The same results were reported by numerous researchers as dissolving the moderate-chain alcohol (C_4-C_8) in the palisade layer of the micelle (very close place in the interface of water and micelle) causing a reduction in electrostatic repulsion of CTA^+[27]. Also, because of the presence of some residual CTAB, silica powder (SC) is more suitable for the adsorption of external ions with pure silica than SCT silica and S silica. Figure 3 illustrates pictures and a schematic for the synthesis of silica particles by the modified Stober method.

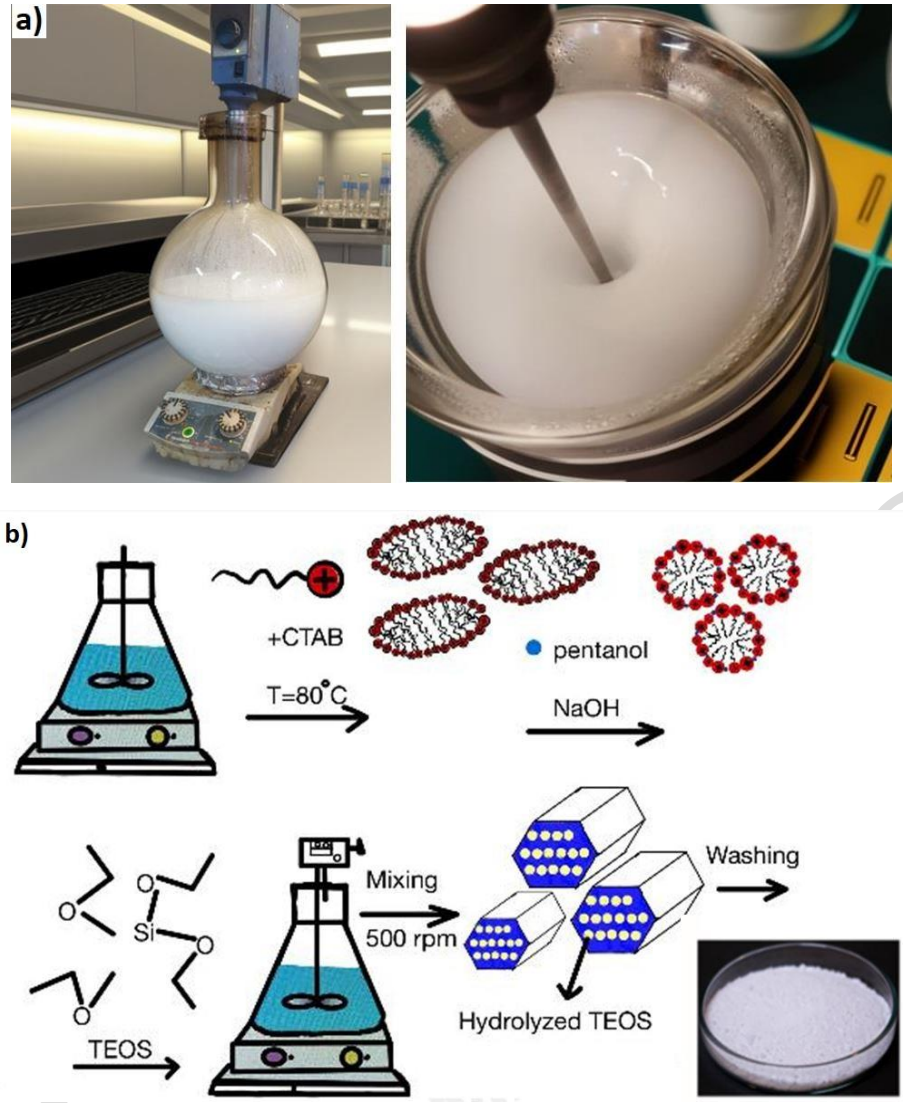

Fig. 3. a:Pictures , b: Schematic for the synthesis of silica particles by modified Stober method

Figure 4 shows the SEM and FESEM images of the S and SCT samples. Accordingly, the presence of CTAB and alcohol not only influences the surface area and the porosity but also affects the morphology of the synthesized particles. CTAB, as a template, leads to the forming of oval-shaped micelles with two cores. By introducing alcohol into the micellar system, it penetrates the palisade layer, and the electrostatic repulsion reduces, consequently reducing micellar aggregation. Hence, the micelles become spherical with

larger dimensions, increasing the pore diameter. Based on the inflation-reduction model, TEOS penetrates the micelles, and then the hydrolyzed $Si(OH)_x$ molecules transfer out of the micelles. According to the SC morphology, it seems that the main reasons for the formation of silica chiral structure by the surfactant are the factors including co-surfactant with suitable chain length (C_4-C_8), reduction of Gibbs free energy for thermodynamic stability (G_s) and flow intensity [28-31].

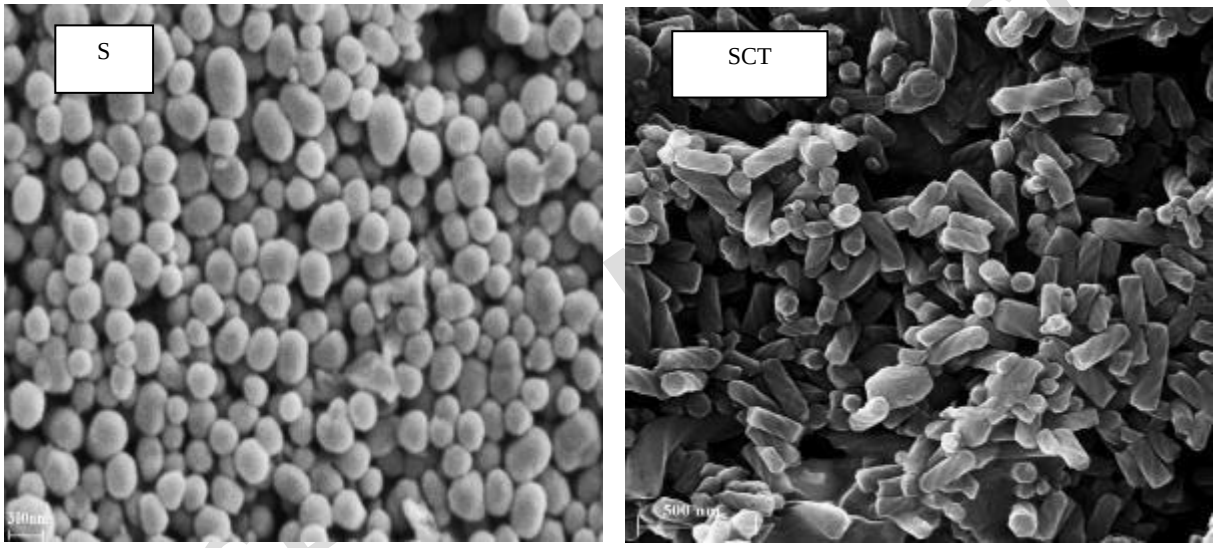

Figure 4. Morphology of S and SCT silica particles, imaged by SEM and FESEM

Figure 5 illustrates the FTIR diagram of the S, SC, and SCT samples. In Figure 5a, which is related to the synthesized silica by the Stober method, the peaks located at 808, 1105, 472, and 1659 cm^{-1} correspond to the symmetric Si-O-Si vibration, asymmetric Si-O-Si vibration, Si-O group vibrations, and the O-H group vibrations, respectively.

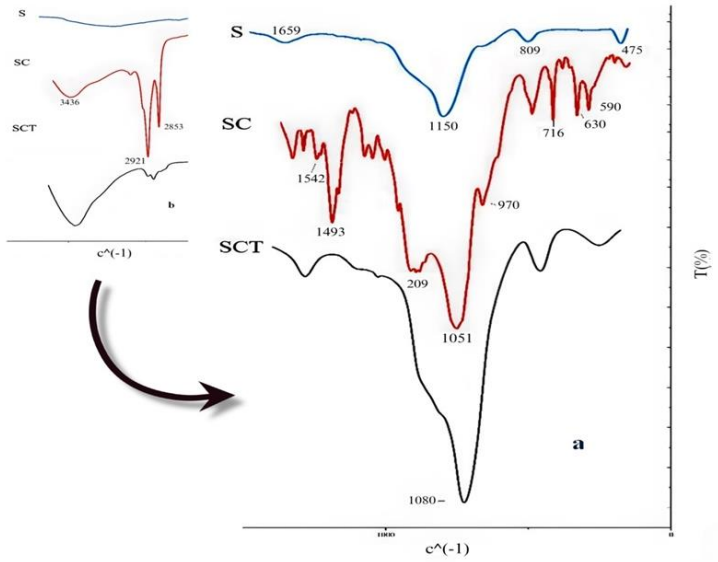

Figure 5. FTIR spectrum for the three silicas S, SC and SCT, at intervals of a) 1600-100 cm^{-1} and b) 3500-2000 cm^{-1}.

The SC sample has two distinct peaks at 2854 cm^{-1} and 2926 cm^{-1}, which correspond to the vibrations of the R=CH_2-CH_3 and -CH_2 alkane groups in the surfactant, respectively. As shown in the figure, the intensity of these peaks is significantly reduced at these points, confirming the removal of large values of surfactant from inside the pores. This reduction in intensity is mainly due to heat treatment, which confirms the successful removal of surfactant from the cavities. In the S sample, the Vibration of the -C=C- group at 1594, 1549, and 968 cm^{-1}, and -CH group at 1494 cm^{-1} and 1219 cm^{-1} are related to the presence of surfactant in synthesized silica that these groups are removed from silica after heat treatment (SCT sample). The characteristic peak of silica, which is related to Si-O-Si, appeared at 1100 cm^{-1}, but the presence of CTAB caused the shift in the peak to 1052 cm^{-1} (SC sample). After heat treatment, this peak again moved to 1100 cm^{-1} (1082 cm^{-1}) and confirmed the removal of a significant value of CTAB.

In the SCT sample, the absence of the 636, 592, and 718 cm^{-1} peaks occurred due to the

removal of the C-Br and C=C groups in the surfactant, respectively. Accordingly, the existing bonds in the cationic surfactant (CTAB) are disappeared after heat treatment and are excreted as carbon dioxide and carbon monoxide. Ultimately, the 3442 cm^{-1} peak is also related to the O-H group in the three samples [32, 33].

3.2. Adsorption of ARS dye by adsorbent

The adsorption operation was performed using three adsorbents (S, SC, and SCT). The S adsorbent has low adsorption due to repulsion between the dye and the adsorbent surface groups and the absence of suitable pores on the surface (<0.01 mg g^{-1}). Also, the adsorption on SCT occurred due to electrostatic attraction and the presence of suitable pores (< 0.1 mg g^{-1}), while a large amount of dye was excreted by washing. For this reason, all adsorption experiments were carried out for Alizarin Res S dye by SC adsorbent due to the appropriate adsorption of anionic dye on the positively charged surface by the CTA^+ functional group and pore structure of the adsorbent surface.

3.3. Effect of contact time on the adsorption of ARS dye on SC adsorbent

In order to study the adsorption of ARS on SC, 0.1 g of SC was utilized for the adsorption of ARS (390mg L^{-1}) at a solution pH of 5.5 and agitation speed of 500 rpm at different time intervals (10, 20, 30, …, 90 min) to attain the equilibrium condition. The amount of ARS adsorbed on the SC was obtained by the below equation:

$$q = \frac{(C_0 - C_e)V}{W} \quad (3)$$

Herein, $\mathbf{q_e}$ is the value of dye adsorption by the adsorbent (mg g^{-1}), $\mathbf{C_e}$ and $\mathbf{C_0}$ are the

residual dye concentration after contact with the dye and the initial dye concentration (mg L^{-1}), respectively. **V** is the total volume (L), and **W** is the value of the adsorbent (g).

According to the experiment results, the adsorption of ARS on the adsorbent increases over time to attain the equilibrium. Figure 6 illustrates the relation between the contact time and the adsorption capacity. The results show that most adsorption occurs at 10 minutes of the adsorption process, and afterward, no significant changes were observed. The amount of ARS that was done in constant conditions (concentration, temperature, adsorbent, pH), adsorbed on SC (q_e), was obtained as 63.72 mg g^{-1}. Also, the adsorption of ARS on SC silica is schematically shown in Figure 7.

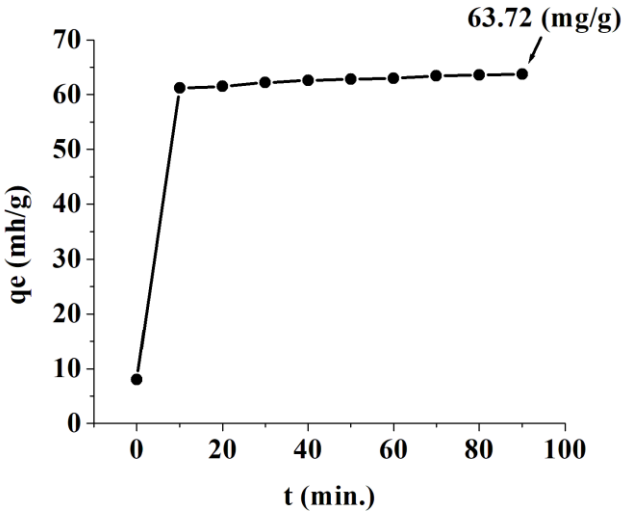

Figure 6. The effect of contact time (min) for the adsorption of ARS on SC adsorbent.

It seems that the adsorption process was occurred by the interaction of positively charged groups on the surface of the porous modified silica (CTA^+) and OH groups of ARS.

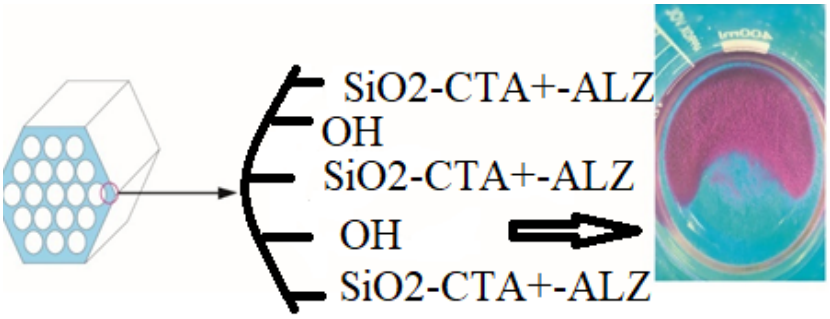

Figure 7. A schematic for the adsorption of ARS on SC.

3.4. Effect of pH on the adsorption of ARS

Various adsorption experiments were conducted at different pH levels ranging from 3 to 13 to determine the optimal pH. The experiments were performed at a temperature of 25°C for 10 minutes, using a dye concentration of 390 mg L^{-1} and an SC dosage of 0.1 g. Results indicate that adsorption occurred more effectively at an acidic pH than a basic pH. The favorable pH range for adsorption was found to be between 3 and 5, with a capacity of 60.58 mg g^{-1} (Figure 8a). Conversely, adsorption at basic pH decreased, with the lowest adsorption observed at a pH of 13 under the same conditions. Additionally, ARS is a suitable variable for pH. As shown in Figures 8b and c, the color hue changes from yellow to red in acidic pH and purple in basic pH.

The zeta potential of SC was measured at different pH levels ranging from 2 to 11 (in increments of 1). The results showed that the isoelectric point of SC lies between pH 4 and 5. Interestingly, dye adsorption remains almost the same due to the minimal differences in the zeta potential observed at pH 3 to 5. Furthermore, the adsorption rate of dye with $(SO_3)^{-2}$ anionic group is highest at acidic pH levels (3 to 5) because of the more positive surface charge. Conversely, when the pH level exceeds 5, the adsorption rate of ARS decreases due to the surface charge becoming more negative.

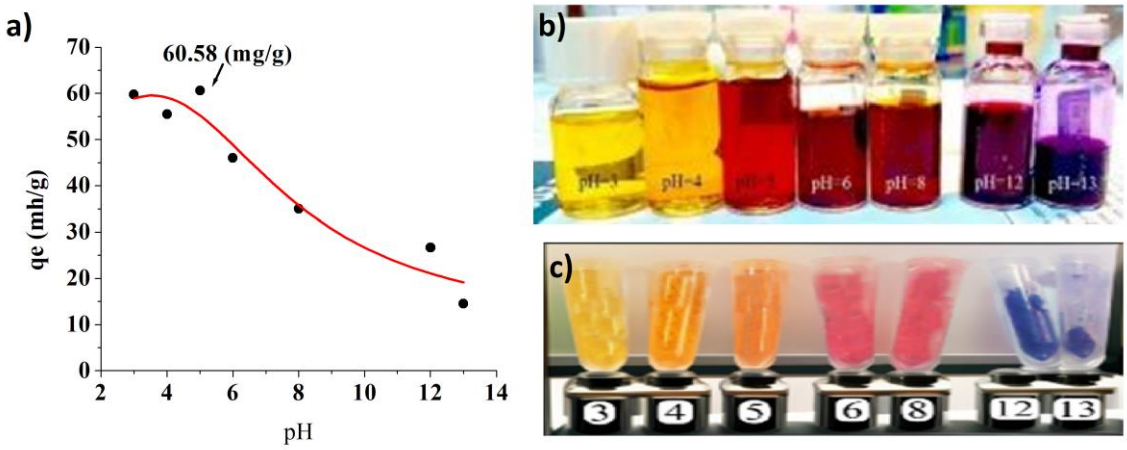

Figure 8. a) Study the adsorption capacity (mg g^{-1}) of ARS on SC at different pHs, b) Color hue changes of ARS dye at different pHs in aqueous medium, c) Color hue changes of ARS dye at different pHsWhen the powders are separated from the liquid and dried at roomtemperature

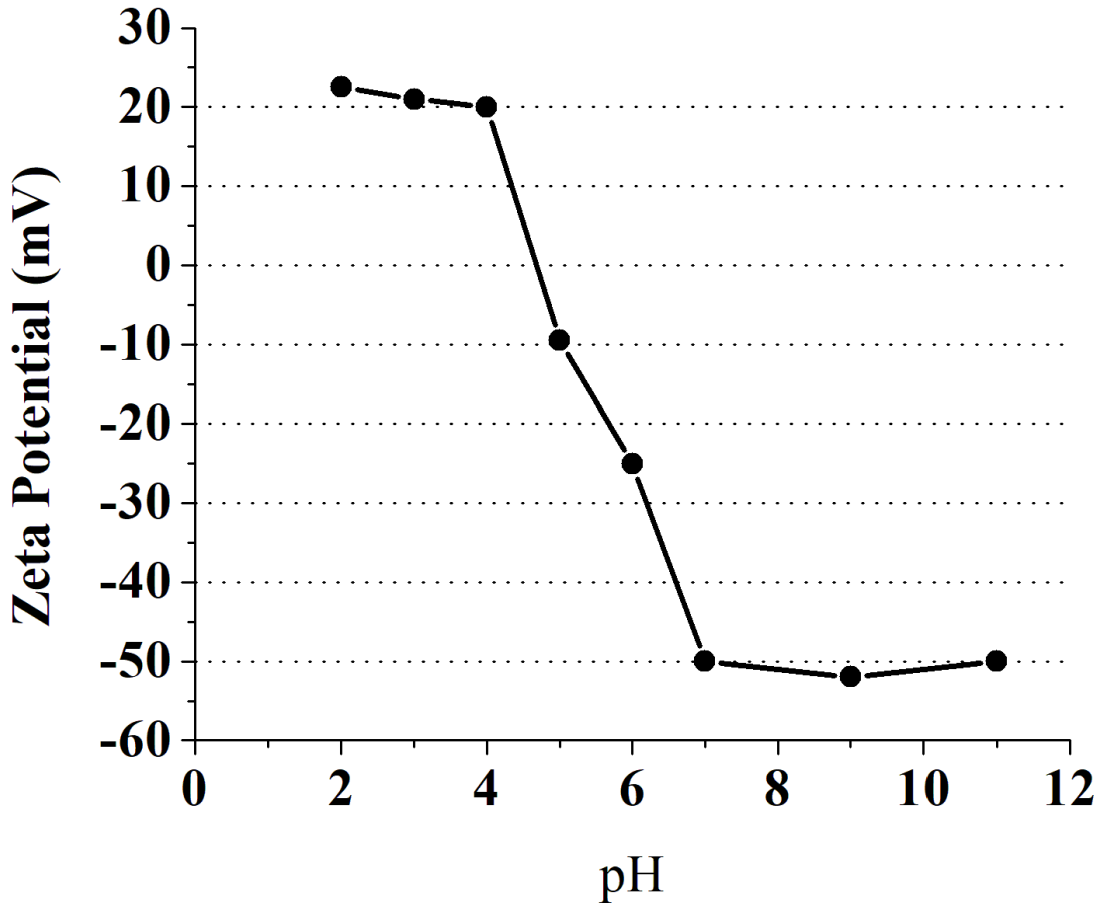

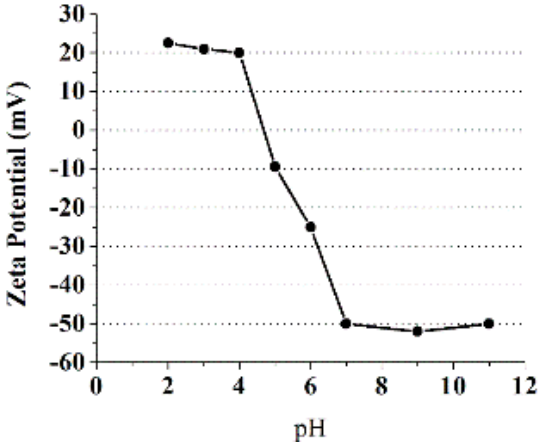

Figure 9. Study the value of zeta-potential in different pHs.

3.5. The effect of ARS initial concentration onthe adsorption

Different concentrations of dye ranging from 290 to 6700 mg/L were analyzed to determine the maximum adsorption capacity of SC absorbent for ARS adsorption. The experiments were conducted with 0.125 g of SC absorbent at a pH of 5.5, ambient temperature, and an agitation speed of 500 rpm. The maximum adsorption capacity of 726.24 mg/g for ARS dye adsorption on silica adsorbent was achieved at a dye concentration of 5000 mg/L. As the concentration of ARS molecules increases, the driving force for adsorption also increases, resulting in higher adsorption by the adsorbent (as shown in Figure 10). Due to equilibrium absorption at high concentrations, experiments and calculations were continued at 390 mg/L.

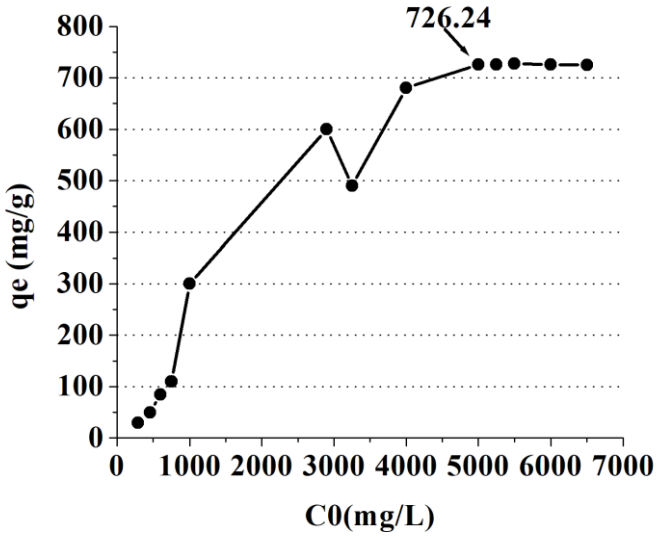

Figure 10. Maximum adsorption capacity ($mg.g^{-1}$) for the adsorption of ARSon SC.

3.6 The effect of adsorbent weight on the adsorption of ARS dye

Figure 11 demonstrates the impact of varying weights of silica powder on the adsorption process. To this end, different quantities of the adsorbent powder (ranging from 0.04 to 0.5 g) were tested at pH = 5.5, ambient temperature, and concentration of 390 mg L^{-1}. The results indicate that dye adsorption reduces with an increase in the amount of adsorbent, which could be attributed to the formation of silica agglomerates at higher values.

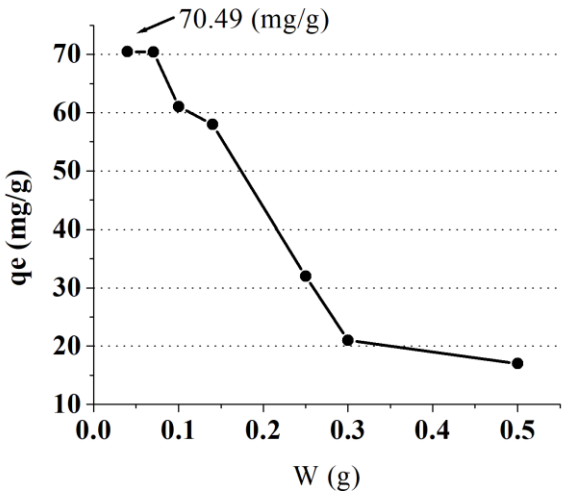

Figure 11. The effect of SC amounts (g) on the adsorption capacity (mg g^{-1}).

3.7. Adsorption isotherms

The adsorption isotherms explain the correlation between the concentration of the adsorbate and the adsorbent in a solution once it reaches equilibrium. Additionally, the adsorption isotherm provides insight into how the adsorbate molecules interact with the adsorbent molecules to reach this equilibrium state. Two models of adsorption isotherms, Langmuir, Freundlich, and Temkin, have been studied to analyze the adsorption of ARS by silica.

3.7.1. Langmuir isotherm

The Langmuir isotherm describes an adsorption process in which the adsorbate molecules are adsorbed equally on all adsorbent sites without any movement. As a result, all molecules have the same enthalpy and activation energy. The Langmuir isotherm can be expressed linearly using the following equation (Eq. 4) [34].

$$\frac{C_e}{q_e} = \frac{1}{K_L Q_0} + \frac{C_e}{Q_0} \quad (4)$$

where **C_e** (mg L^{-1}) and q_e (mg g^{-1}) are the concentration and adsorption at equilibrium mode, respectively. The maximum adsorption value is defined as q_m (mg g^{-1}), and also Langmuir equilibrium constant is k_L(l mg^{-1}). Also, the dimensionless constant, known as the separation factor (R_L), is defined in the Langmuir isotherm which is defined by Webber and ChackraWortti (Eq. 5) [35].

$$R_L = \frac{1}{1+K_L C_e} \quad (5)$$

3.7.2. Freundlich isotherm

The Freundlich isotherm was the first model developed to explain reversible non-ideal adsorption. This model is used to study monolayer adsorption and can describe homogeneous and multilayer systems with non-uniform enthalpy distributions. The isotherm works on the principle that sites with stronger bonds get filled earlier, followed by the filling of other sites. Additionally, the adsorption process reduces exponentially until it is completed. The equation is expressed as (Eq. 6) [10, 36].

$$\log q_e = \log K_F + \frac{1}{n} \log C_e \quad (6)$$

where **k_f**(l mg^{-1}) and **1/n** are the equilibrium constant and adsorption intensity, respectively.

3.7.3. Temkin isotherm

Temkin isotherm is another isotherm that represents the interaction ofadsorbate and adsorbent and is expressed as (Eqs. 7 and 8) [37, 38]:

$$q_e = B \ln A + B \ln C_e \quad (7)$$

Where: $B = \frac{RT}{b}$ (8)

Table 2 presents the parameters obtained from the Langmuir, Freundlich, and Temkin isotherms. The regression coefficients (R2) for the Langmuir, Freundlich, and Temkin isotherms are 0.99, 0.96, and 0.98, respectively. By comparing the values of these isotherms, we can conclude that the Langmuir isotherm is a better fit for describing the absorption of ARS on silica than the Freundlich and Temkin isotherms. We also calculated the separation factor (R_L = 0.00048) and found that the adsorption process is highly desirable. As the number tends to zero, the process moves towards irreversibility. Figure 12 displays the graphs of the three isotherms (Langmuir, Freundlich, and Temkin).

Table 2. The values of Langmuir, Freundlichand Temkinisotherms for the adsorption of ARS on SC.

Langmuir constants			**Freundlich constants**			**Temkin constants**		
K_l ($L.mg^{-1}$)	**q_m ($mg.g^{-1}$)**	**R^2**	**k_f ($mg^{1+n}.g.L^n$)**	**1/n**	**R^2**	**A**	**B**	**R^2**
0.172	68.96	0.99	41.68	0.9	0.97	0.176	19.55	0.98

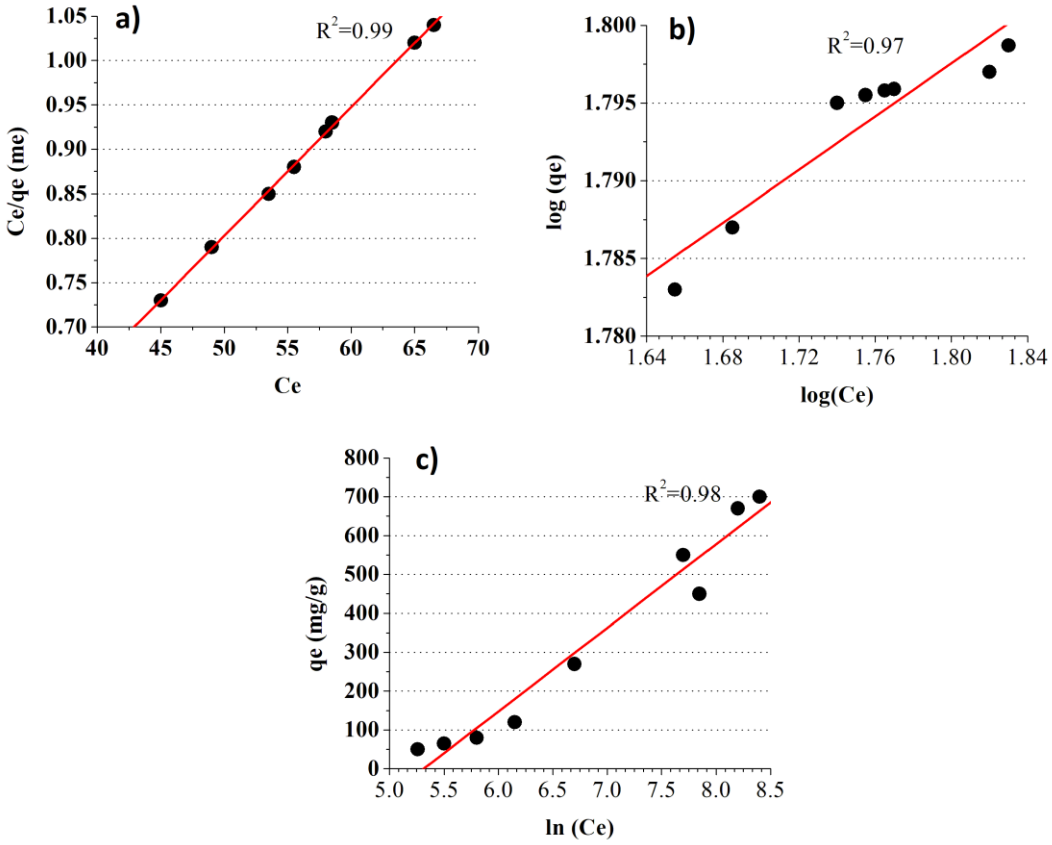

Figure 12. Graphs of three a) Langmuir, b) Freundlich and c) Temkin isotherms

3.6. Adsorption kinetics of ARS dye on SC

This study reviews the adsorption kinetics of ARS dye on SC. The optimal time for dye adsorption on the adsorbent is defined as the appropriate time, after which the adsorption rate remains constant. The adsorption kinetics of dye on SC were investigated under optimum conditions, including ambient temperature, 0.125 g adsorbent dosage, 390 mg L^{-1} initial dye concentration, 5.5 pH of solution, and 500 rpm agitation speed. The adsorption kinetics were examined at various intervals (10, 20, 30, ..., 90 min) to determine the equilibrium time. The kinetics adsorption of ARS on the adsorbent was examined using the pseudo-first-order and pseudo-second-order models.

3.7.1. Pseudo-first-order kinetic

The pseudo-first-order kinetic model illustrates the relationship between reaction speed and concentration as below equation (Eq. 9) [39]:

$$\log(q_e - q_t) = \log(q_e) - \frac{k_1}{2.303} t \qquad (9)$$

As, K_1 (min^{-1}) is the constant of the pseudo-first-order equation and q_t (mg g^{-1}) is the dye adsorption capacity at time t.

3.7.2. Pseudo-second-order kinetic

Pseudo-second-order kinetic model is defined the adsorbent surface as the adsorption limiting factor and describe as follows (Eq. 10) [40]:

$$\frac{t}{q_t} = \frac{1}{kq_e^2} + \frac{1}{q_e} t \qquad (10)$$

where, k_2 (g $mgmin^{-1}$) is the constant of the pseudo-second-order kinetic equation. Table 3 displays the kinetic values of two equations used to study the adsorption of ARS by silica sorbent. The R-squared regression constant for the pseudo-first-order and pseudo-second-order kinetics models are 0.8 and 0.99, respectively, as shown in the table. This indicates that the adsorption of ARS by silica sorbent follows the pseudo-second-order kinetics. Figure 13 illustrates the plots of the two kinetics models: Pseudo-first-order and Pseudo-second-order.

Table 3. The kinetics values for the adsorption of ARS on SC.

Pseudo-first-order kinetic				**Pseudo-second-order kinetic**		
$q_{e(cal)}$ ($mg.g^{-1}$)	**$q_{e(exp)}$ ($mg.g^{-1}$)**	**K_1 (min^{-1})**	**R^2**	**$q_{e(cal)}$ ($mg.g^{-1}$)**	**K_2 ($g.mg^{-1}.min^{-1}$)**	**R^2**

50.1	59.1	0.0004	0.8	60.97	0.032	0.99

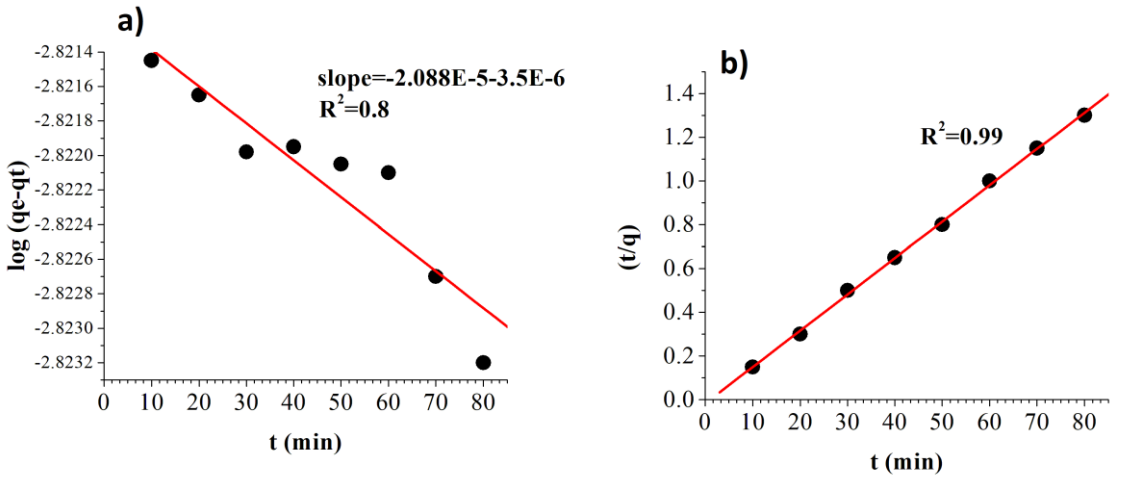

Figure 13. Plots of a) Pseudo-first-order and b) Pseudo-second-order kinetics.

3.8. Thermodynamic studies

In order to determine the optimal temperature for adsorption, the effect of temperature was studied within the range of 298-335K under constant conditions. Temperature is a crucial factor in the adsorption process, and to investigate its impact, some experiments were conducted at a pH of 5.5, a concentration of 390 mg L-1, and an adsorbent content of 0.125 g. The temperature range of the experiments was 298-335K. The thermodynamic parameters were defined as follows (Eqs. 11-13) [41]:

$$\Delta G^\circ = \Delta H^\circ - T\Delta S^\circ \quad (11)$$

$$K_C = \frac{C_A}{C_S} \quad (12)$$

$$LnKc = \frac{\Delta S^\circ}{R} - \frac{\Delta H^\circ}{RT} \quad (13)$$

ΔG° (kJ mol^{-1}) and ΔH° (kJ mol^{-1}) arethe Gibbs free energy and enthalpy, respectively. Also, entropy ΔS° (kJ mol^{-1} K^{-1}) could be studied by equilibrium constant (K_C). C_A is the

adsorbed dye on SC (mol L^{-1}) and C_S is the solutiondye concentration atequilibrium (mol L^{-1}).

The straight plot of lnKC versus T^{-1} is presented in Figure 14. The thermodynamic constants are shown in Table 4. The positive values of ΔH suggest that the adsorption process is endothermic. Additionally, the negative values of ΔS, which accompany the endothermic process, result in positive values of ΔG, indicating a nonspontaneous process.

Table 4. Thermodynamics parameters for the adsorption of ARS on SC.

T(k)	ΔG°(kJ mol^{-1})	ΔH° (kJ mol^{-1})	ΔS° (kJ mol^{-1} K^{-1})
298	3.81893	3.334	-0.00174
308	4.66681		
318	5.42015		
328	5.76445		
335	6.88402		

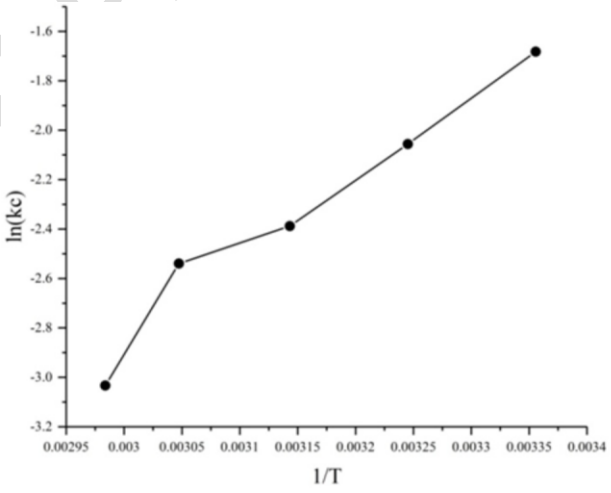

Figure 14. Thermodynamic study for the adsorption of ARS on SC adsorbent.

3.9. Study the binding of ARS on SC by adsorption

In order to understand how ARS binds to the adsorbent, we conducted an FTIR analysis to examine the interaction between the dye and the adsorbent. Figure 15 displays the FTIR spectra of ARS, pure silica (SC), and the adsorbed dye on the adsorbent (ARS-SC). The FTIR spectrum revealed a peak shift indicating the presence of the Si-O-CH_3 chemical group, which is responsible for the physical bonds between the cationic surfactant and the silica powder. Additionally, SC became an appropriate powder for adsorbing anionic dye by creating this bond and positive sites on the surface of silica. The asymmetric stretching vibration was observed at 3800-3000 cm^{-1} for all three samples of SC, ARS, and ARS-SC.

The H-C vibration at 2850-2920 cm^{-1} indicates the presence of the alkane group and confirms the existence of CTAB in both SC and ARS-SC samples. Additionally, the methyl and methylene groups in the CTAB are also vibrated at 1440-1490 cm^{-1}, which may be related to the presence of an aromatic ring in the ARS structure. The vibration at 730-700 cm^{-1} is also related to the Ar-Si-O-CH_3 chemical group. The peak shift at the SC sample from 1400 to 1348 cm^{-1} represents the vibration of the C-H and OH chemical groups, indicating the establishment of a chemical bond between ARS and SC.

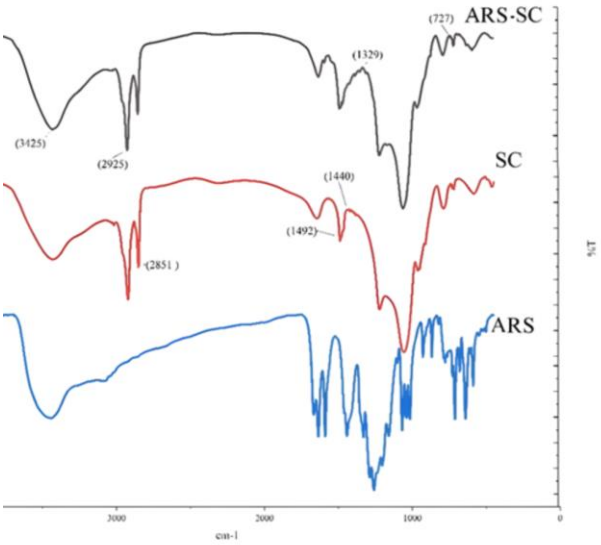

Figure 15. FTIR spectra of a) ARS, b) SC and c) ARS-SC.

3.10. Study the metal ion adsorption By ARS-SC hybrid

As previously discussed, hybrid pigments effectively eliminate heavy metal ions. To achieve this, SC-ARS adsorbent is utilized to remove heavy metals such as Pb^{2+}, Cd^{2+}, and Cu^{2+}. The results of removing these three heavy metal ions on SC and ARS-SC, as obtained by the ICP instrument, are presented in Table 5. Although synthesized silica through the modified Stober method can remove large amounts of dye due to its negative sites and proper pore, the removal of heavy metal ions by SC adsorbent is less effective than ARS-SC due to the presence of positive sites on the surface.

When the ARS dye binds to the positive site on the silica, it reduces the number of positive sites on the silica surface. As a result, the amount of negative charge on the silica surface increases, which can be very helpful in removing heavy metal ions.

Based on the ICP results, there is no significant difference in the removal of Cu (II) heavy metal by SC and SC-ARS. Hybrid materials are only 0.6% more efficient than pure

silica. However, the difference between the two sorbents is pronounced when removing the other two metals. The removal percentage of Cd (II) ions by SC and ARS-SC is about 42.7% and 84.1%, respectively. This means that more negative sites increase the removal of Cd (II) ions by 41%. The best result is related to removing heavy metal Pb (II). The SC silica removed about 47.2% of heavy metal Pb (II), whereas the ARS-SC hybrid removed 99.87%. Thus, SC-ARS increased removal efficiency by 52.6%.

This hybrid material has several advantages over its components, such as ease of synthesis and changing the color of dye by changing pH, which can be used to design a sensor for detecting heavy metal. For example, by adding ARS-SC to an unknown Cu (II) sample, the color changes to light pink. It also easily collects the adsorbent after heavy metal removal. Figure 16 illustrates a comparison of removing the three heavy metals of Pb (II), Cu (II), and Cd (II).

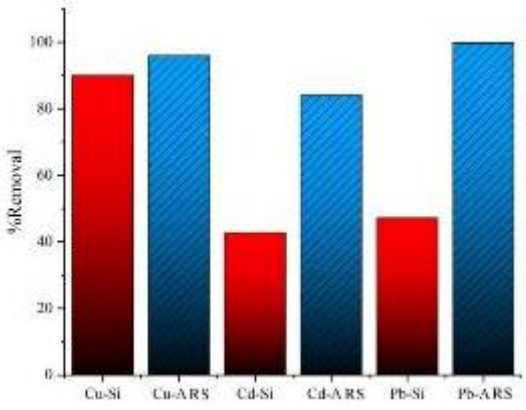

Figure 16. Comparison of removing the three heavy metals of Pb (II), Cu (II) and Cd (II)

3.11. Thermal stability of SC-ARS hybrid

The TGA/DTG analysis was conducted to assess the thermal stability enhancement of the ARS-SC hybrid pigment compared to its individual organic and inorganic components. After chemical bonding between ARS dye and porous silica, the thermal stability of

ARS-SC was investigated in comparison to SC and ARS at different weight loss percentages (Figure 17). During TGA/DTG analysis, a sample containing 84 mg g^{-1} of ARS dye was tested. The spectra of SC, ARS-SC, and ARS were compared at $T_{15\%}$, $T_{30\%}$, and $T_{40\%}$. At $T_{7\%}$, weight loss was observed for SC, SC-ARS, and ARS due to the removal of water at 168°C, 126°C, and 275°C, respectively. The degradation temperatures of SC, ARS-SC, and ARS ($T_{15\%}$) were found to be 172°C, 190°C, and 334°C, respectively.

The results of the study showed that the hybridized sample (ARS-SC) had increased thermal stability at $T_{15\%}$ compared to SC and ARS by approximately 18 ˚C and 5 ˚C, respectively. At $T_{30\%}$, the degradation temperatures for SC, SC-ARS, and ARS samples were found to be 225 ˚C, 245 ˚C, and 354 ˚C, respectively. The ARS-SC sample was observed to be more stable than pure SC and pure ARS, with a difference of 20 and 10 °C, respectively.

At $T_{40\%}$, the degradation temperature of three materials was measured. The materials were SC, ARS-SC, and ARS. The degradation temperature of SC was 257 °C, the degradation temperature of ARS-SC was 288 °C, and the degradation temperature of ARS was 364 °C. This indicates that the thermal stability of ARS-SC was increased by about 31 and 22 °C compared to SC and ARS, respectively.

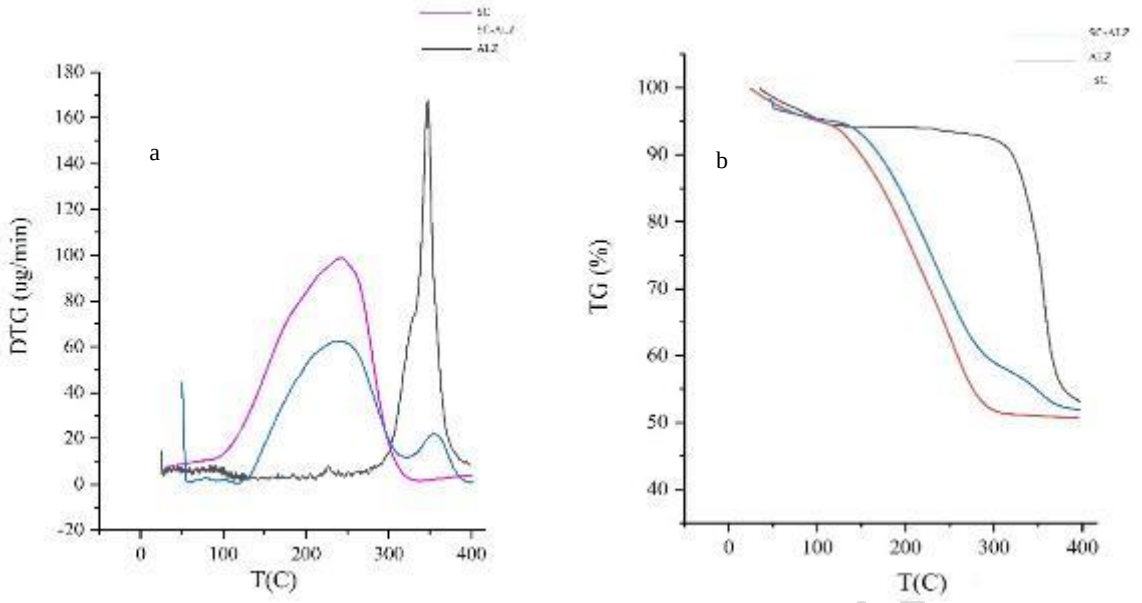

Figure 17. a) TGA and b) DTG for SC, ARS and SC-ARS.

Table 5. Weight loss at different temperature for SC, ARS and ARS-SC.

sample	$T_{7\%}$ (°C)	$T_{15\%}$ (°C)	$T_{30\%}$ (°C)	$T_{40\%}$ (°C)
SC	168	172	225	257
SC-ARS	126	190	245	288
ARS	275	334	354	364

4. Conclusion

In recent years, hybrid pigments have been introduced to promote the characteristics and benefits of organic materials and minerals, as well as to decrease the weaknesses and defects of each component. In this study, the mineral substances with high pores and high specific surface area was prepared by the modified Stober method applying cationic surfactant (CTAB). Using this method, amorphous powder is synthesized with a specific surface area of 1174 m^2/g, pore diameter of 4.09 nm, very high adsorption and helical morphology and use as the mineral part of hybrid material. Then, ARS dye was used as

an adsorbent for the adsorption of heavy metal ions after making bond to the mineral part and increasing the thermal stability of the hybrid dye towards the pure dye. Meantime, the operational condition including the initial dye concentration, temperature, adsorbent amount and pH was studied as well as the adsorption kinetics of ARS dye by silica sorbents. According to the results, the best consequences was obtained for the adsorption of5 g $L^{-1}$of dye with 0.04 g of adsorbent at pH 5 for 10 min at 25° C and the maximum adsorption capacity was obtained as 726.24 mg g^{-1}. Also, the adsorption process wasbest fitted to the Langmuir adsorption isotherm and pseudo-second-order adsorption kinetics. Furthermore,the adsorption ability of synthesized material (ARS-SC) was tried for the removal of three metal ions namelyPb^{2+}, $Cd^{2+}$and Cu^{2+} from their metal salts. ICP results indicated thatARS-SCwas able to removeCu^{2+}, Cd^{2+}, and Pb^{2+} ions from the aqueous medium up to 96%, 84% and 99%, respectively. TG/DTG experiments was applied under oxygen to assess the thermal stability. According to the results, the presence of CTAB surfactant made the prepared hybrid more stable by approximately 23° C. Also, this hybrid is 12° C more thermally stable than the pure ARS dye.

5. References

[1]. Khan FS, Mubarak NM, Tan YH, Khalid M, Karri RR, Walvekar R, Abdullah EC, Nizamuddin S, Mazari SA. A comprehensive review on magnetic carbon nanotubes and carbon nanotube-based buckypaper for removal of heavy metals and dyes. J Hazardous Mater. 2021; 413:125375. http://dx.doi.org/10.1016/j.jhazmat.2021.125375

[2]. Sheth Y, Dharaskar S, Khalid M, Sonawane S. An environment friendly approach for heavy metal removal from industrial wastewater using chitosan based biosorbent: A

review. Sustain Energy Technol Asses. 2021; 43:100951. http://dx.doi.org/10.1016/j.seta.2020.100951

[3] Razmara Z, Eigner V, Dusek M. Hydrothermal synthesis and crystal structure of a new organic-inorganic magnesium complex for the removal of tetracycline. J Mol Struct. 2021; 1224:129315. http://dx.doi.org/10.1016/j.molstruc.2020.129315

[4] Ahmad N, Sereshti H, Mousazadeh M, Nodeh HR, Kamboh MA, Mohamad S. New magnetic silica-based hybrid organic-inorganic nanocomposite for the removal of lead (II) and nickel (II) ions from aqueous solutions. Mater Chem Phys. 2019; 226:73-81. http://dx.doi.org/10.1016/j.matchemphys.2019.01.002

[5]. Wei J, Duan L, Wei J, Hoffmann E, Song Y, Meng X. Lead removal from water using organic acrylic amine fiber (AAF) and inorganic-organic P-AAF, fixed bed filtration and surface-induced precipitation. J Environ Sci. 2021; 101:135-44., http://dx.doi.org/10.1016/j.jes.2020.08.009

[6] Wu J, Wang T, Wang J, Zhang Y, Pan WP. A novel modified method for the efficient removal of Pb and Cd from wastewater by biochar: Enhanced the ion exchange and precipitation capacity. Sci Total Enviro. 2021; 754:142150. http://dx.doi.org/10.1016/j.scitotenv.2020.142150

[7]. Efome JE, Rana D, Matsuura T, Lan CQ. Effects of operating parameters and coexisting ions on the efficiency of heavy metal ions removal by nano-fibrous metal-organic framework membrane filtration process. Sci Total Environ. 2019; 674:355-62. http://dx.doi.org/10.1016/j.scitotenv.2019.04.187

[8] Araucz K, Aurich A, Kołodyńska D. Novel multifunctional ion exchangers for metal ions removal in the presence of citric acid. Chemosphere. 2020; 251:126331. http://dx.doi.org/10.1016/j.chemosphere.2020.126331

[9] De Almeida Lopes TS, Hessler R, Bohner C, Junior GB, de Sena RF. Pesticides removal from industrial wastewater by a membrane bioreactor and post-treatment with either activated carbon, reverse osmosis or ozonation. J Environ Chem Eng. 2020; 8(6):104538. http://dx.doi.org/10.1016/j.jece.2020.104538

[10]. Sheshdeh RK, Nikou MR, Badii K, Limaee NY, Golkarnarenji G. Equilibrium and kinetics studies for the adsorption of Basic Red 46 on nickel oxide nanoparticles-modified diatomite in aqueous solutions. Journal of the taiwan institute of chemical Engineers. 2014; 45(4):1792-802. http://dx.doi.org/10.1016/j.jtice.2014.02.020

[11] Wang Y, Zhou R, Wang C, Zhou G, Hua C, Cao Y, Song Z. Novel environmental-friendly nano-composite magnetic attapulgite functionalized by chitosan and EDTA for cadmium (II) removal. J Alloy Comp. 2020; 817:153286.. http://dx.doi.org/10.1016/j.jallcom.2019.153286

[12]. Davodi B, Ghorbani M, Jahangiri M. Adsorption of mercury from aqueous solution on synthetic polydopamine nanocomposite based on magnetic nanoparticles using Box–Behnken design. J Taiwan Instut Chem Eng. 2017; 80:363-78.. http://dx.doi.org/10.1016/j.jtice.2017.07.024

[13]. Badsha MA, Khan M, Wu B, Kumar A, Lo IM. Role of surface functional groups of hydrogels in metal adsorption: From performance to mechanism. J Hazard Mater. 2021; 408:124463. http://dx.doi.org/10.1016/j.jhazmat.2020.124463

[14]. Xie N, Wang H, You C. Role of oxygen functional groups in Pb2+ adsorption from aqueous solution on carbonaceous surface: A density functional theory study. J Hazard Mater. 2021; 405:124221. https://doi.org/10.1016/j.jhazmat.2020.124221

[15] El-Hallag I, Al-Owais A, El-Mossalamy ES. Kinetic and thermodynamic investigation of the removal of alizarin red dye using silica-supported nanoscale zero-valent iron particles. Sci Report. 2025; 15(1):31461. https://doi.org/10.1038/s41598-025-15233-z

[١٦] Wei X, Liu J, Yan H, Li T, Wang Y, Zhao Y, Li G, Zhang G. Synthesis of large mesoporous silica for efficient CO_2 adsorption using coal gasification fine slag. Separat Purif Technol. 2025; 353:128348. https://doi.org/10.1016/j.seppur.2024.128348

[17] Barman MK. Recent advancements of silica supported hybrid composite materials and its application for heavy and toxic metal ion removal: a review. Geomicrobiol J. 2026; 43(4):387-409. https://doi.org/10.1080/01490451.2025.2592147

[18]. Hoshyar SA, Barzani HA, Yardım Y, Şentürk Z. The effect of CTAB, a cationic surfactant, on the adsorption ability of the boron-doped diamond electrode: Application for voltammetric sensing of Bisphenol A and Hydroquinone in water samples. Colloid Surf A: Physicochem Eng Aspect. 2021; 610:125916. https://doi.org/10.1016/j.colsurfa.2020.125916

[19]. Abdelsamad AM, Saeidi N, Mackenzie K. Mesoporous silica nanoparticles for rapid removal of PFOA: Impact of surface functional groups on adsorption efficiency and adsorbent regeneration. Environmen Poll. 2025; 383:126796. https://doi.org/10.1016/j.envpol.2025.126796

[20]. Zaggout FR, Qarraman AE, Zourab SM. Behavior of immobilized Alizarin Red S into sol–gel matrix as pH sensor. Mater Lett. 2007; 61(19-20):4192-5. https://doi.org/10.1016/j.matlet.2007.01.080.

[21]. Li D, Liu Q, Ma S, Chang Z, Zhang L. Adsorption of alizarin red S onto nano-sized silica modified with γ-aminopropyltriethoxysilane. Adsorp Sci Technol. 2011; 29(3):289-300. https://doi.org/10.1260/0263-6174.29.3.289

[22]. Li Y, Zhang L, Han H, Tian X, Shi X, Wang K, Zhang S. Preconcentration of ultra-trace Cu (II) and Cd (II) using SPE based on an alizarin complexone modified silica gel with detection using FAAS and determination of ultra-trace Cu (II) by the naked eye. Anal Method. 2015; 7(9):3876-82. https://doi.org/ 10.1039/C4AY03114H

[23]. Ibrahim IA, Zikry AA, Sharaf MA. Preparation of spherical silica nanoparticles: Stober silica. J Am Sci. 2010;6(11):985-9.

[24]. Kruk M, Jaroniec M, Kim JM, Ryoo R. Characterization of highly ordered MCM-41 silicas using X-ray diffraction and nitrogen adsorption. Langmuir. 1999; 15(16):5279-84. https://doi.org/ 10.1021/la990179v

[25]. Sangwichien C, Aranovich GL, Donohue MD. Density functional theory predictions of adsorption isotherms with hysteresis loops. Colloid Surf A: Physicochem Eng Aspect. 2002; 206(1-3):313-20. https://doi.org/ 10.1016/S0927-7757(02)00048-1

[26]. Musić S, Filipović-Vinceković N, Sekovanić L. Precipitation of amorphous SiO_2 particles and their properties. Brazilian J Chem Eng. 2011; 28(1):89-94. https://doi.org/10.1590/S0104-66322011000100011

[27]. Liu W, Chen Y, Hao H, Zhang K, Zhang H, Teng H. The significant effects of linear medium chain fatty alcohols on phase behavior of aqueous solution of mixed

cationic–anionic surfactant. J Dispersion Sci Technol. 2019; 40(2):299-305. https://doi.org/ 10.1080/01932691.2018.1468261

[28] Zhang Q, Lü F, Li C, Wang Y, Wan H. An efficient synthesis of helical mesoporous silica nanorods. Chem Lett. 2006; 35(2):190-1. https://doi.org/ 10.1246/cl.2006.190

[29] Yang S, Zhao L, Yu C, Zhou X, Tang J, Yuan P, Chen D, Zhao D. On the origin of helical mesostructures. J Am Chem Soc. 2006; 128(32):10460-6. https://doi.org/ 10.1021/ja0619049

[30]. Gök Y, Gök HZ. Synthesis, characterization and catalytic performance in enantioselective reactions by mesoporous silica materials functionalized with chiral thiourea-amine ligand. Res Chem Intermed. 2021; 47(2):853-74. https://doi.org/10.1007/s11164-020-04301-w

[31]. Wang J, Wang W, Sun P, Yuan Z, Li B, Jin Q, Ding D, Chen T. Hierarchically helical mesostructured silica nanofibers templated by achiral cationic surfactant. J Mater Chem. 2006; 16(42):4117-22. https://doi.org/10.1039/b609243h

[32] Coates J. Interpretation of infrared spectra, a practical approach. Encycl Anal Chemistry. 2000;12:10815-37. https://doi.org/ 10.1002/9780470027318.a5606

[33]. Araghi M, Ghahari M, Afarani MS. Synthesis and investigation of antimicrobial properties of SiO_2@ Cu rods with core–shell structure. Journal of environmental chemical engineering. 2017; 5(2):1780-90. https://doi.org/ 10.1016/j.jece.2017.03.012

[34]. Limaee NY, Rouhani S, Olya ME, Najafi F. Selective 2, 4-dichlorophenoxyacetic acid optosensor employing a polyethersulfone nanofiber-coated fluorescent molecularly imprinted polymer. Polymer. 2019; 177:73-83. https://doi.org/10.1016/j.polymer.2019.05.067

[35]. Weber TW, Chakravorti RK. Pore and solid diffusion models for fixed-bed adsorbers. AIChE J. 1974; 20(2):228-38. https://doi.org/10.1002/aic.690200204

[36]. Limaee NY, Rouhani S, Olya ME, Najafi F. Selective recognition of herbicides in water using a fluorescent molecularly imprinted polymer sensor. J Fluores. 2020; 30(2):375-87. https://doi.org/10.1007/s10895-020-02508-z

[38]. Arami M, Limaee NY, Mahmoodi NM. Investigation on the adsorption capability of egg shell membrane towards model textile dyes. Chemosphere. 2006; 65(11):1999-2008. https://doi.org/10.1016/j.chemosphere.2006.06.074

[38]. Kalhor MM, Rafati AA, Rafati L, Rafati AA. Synthesis, characterization and adsorption studies of amino functionalized silica nano hollow sphere as an efficient adsorbent for removal of imidacloprid pesticide. J Mol Liquids. 2018; 266:453-9. https://doi.org/10.1016/j.molliq.2018.06.041

[39]. Raju CA, Babu KS. Studies on Biosorption of Methyl Red Dye With Pterocladia Lucida Powder and Optimization Throught Central Composite Design.

[40]. Arami M, Limaee NY, Mahmoodi NM. Evaluation of the adsorption kinetics and equilibrium for the potential removal of acid dyes using a biosorbent. Chem Eng J. 2008; 139(1):2-10. https://doi.org/10.1016/j.cej.2007.07.060

[41] Asuha S, Fei F, Wurendaodi W, Zhao S, Wu H, Zhuang X. Activation of kaolinite by a low-temperature chemical method and its effect on methylene blue adsorption. Powder Technol. 2020; 361:624-32. https://doi.org/ 10.1016/j.powtec.2019.11.068